Assessing High-Order Harmonic Resonance in Locomotive-Network Based on the Impedance Method

JING LI [ID]1, (Student Member, IEEE), MINGLI WU1, (Member, IEEE), MARTA MOLINAS [ID]2, (Member, IEEE), KEJIAN SONG1, (Member, IEEE), AND QIUJIANG LIU1

1 School of Electrical Engineering, Beijing Jiaotong University, Beijing 100044, China
2 Department of Engineering Cybernetics, Norwegian University of Science and Technology, 7034 Trondheim, Norway

Corresponding authors: Kejian Song (kjsong@bjtu.edu.cn) and Mingli Wu (mlwu@bjtu.edu.cn)

ABSTRACT Many new types of locomotives are put to use in electric railway systems, resulting in instability problems such as high-order harmonic resonance occurring as a consequence of the interaction between the electrical locomotive (including electrical multiple units) and the traction network. In order to investigate this problem, this paper adopts the impedance-based approach to analyze the stability properties of the system interaction. The detailed impedance of the traction network is obtained by taking its distributed parameters into account. Then the locomotive converter with single-phase transient current control algorithm (TCCA), which can represent the locomotive when performing the impedance-based stability analysis, is modeled as the *dq*-frame impedance by single-phase *dq* decomposition. By plotting bode diagrams of the impedance for the traction network and the locomotive separately, and calculating the phase margin at the intersection point of the magnitude of the two impedances, the stability of the locomotive-network system is evaluated and thus the high-order harmonic resonance can be predicted. Moreover, a time-domain model of locomotive-network systems is established in this paper, which can reproduce the high-order harmonic resonance in the time domain as a first validation step of the analysis. Finally, a field test in a traction substation of the Beijing-Harbin Railway is carried out to finally validate the effectiveness of the proposed method. The stability analysis method in this paper is simple and effective without the need for a complex calculation of some norms or Eigenvalues. As a result, the high-order harmonic resonance can be predicted before a new type of locomotive is put into use.

INDEX TERMS Electric railway, stability, high-order harmonic resonance, impedance, locomotive, traction network, bode diagram.

I. INTRODUCTION

To meet the requirements for large volume and high efficiency in electric railways, more and more new types of trains with AC-DC-AC traction drive systems, such as high-power locomotives and electric multiple units (hereafter, all referred to as locomotives), are put into use. The traction network provides electric power for these locomotives, which forms an interacted locomotive-network (L-N) system. The locomotives' power electronic converters introduce nonlinearity into the traction networks, adding more complication to the interaction relationship between the locomotives and traction networks. The interaction may result in instability problems in L-N systems when different locomotives connect to different traction networks [1]. One of the instability phenomena is high-order harmonic resonance (HOHR) which frequently occurs when locomotives are running on the railway [2]. The instability problems are harmful to not only the power supply of the traction network but also to the control systems of the locomotive. Consequently, to guarantee the safety of the running locomotives, it is necessary to assess the instability problems so that they can be predicted.

The stability of L-N systems is essentially influenced by the interaction between the locomotives and the

The associate editor coordinating the review of this manuscript and approving it for publication was Firuz Zare.

traction networks. Seen from the traction network side, in previous literature [3], [4] the converter in the locomotive running on the railway is usually regarded as a harmonic current source. Studies have shown that the input admittance of the converter in the locomotive can affect the traction network analysis, thereby causing the instability problem [5], [6]. While seen from the locomotive side, the traction network is usually modeled as an equivalent resistance-inductance in series circuit [7], [8]. In fact, the traction network has a distributed structure which is cascaded with the locomotive, thereby resulting in the instability problem [9], [10]. Therefore, to analyze the stability of the L-N system, both the linearization of the single-phase converter and the distributed structure of the traction network should specifically be considered.

The stability of the L-N system has been investigated to some extent. Some research presents the instability phenomena through an analysis of field test data [11]. In [12], the time-domain model of the L-N system is established in order to simulate the instability problems. To analyze the stability of the L-N system in a systematic way, the theoretical model of a locomotive converter is derived in [13]–[15] and the system stability is then evaluated through stability criteria. In addition, the influence of controller parameters on system stability is discussed. Thereafter, different suppression methods are proposed to mitigate the instability phenomena [2], [16], but these measures could not completely resolve the instability problems of all the different L-N systems.

The present research of L-N system stability is, however, still insufficient, as explained below:

(1) There are various types of locomotives which have different control strategies and electrical parameters. It is necessary to study the impedance models of different types of locomotives.

(2) The traction network has an impact on the stability of the L-N system and the actual distributed structure should be considered when the impedance model is derived.

(3) The stability characteristics differ in different L-N systems. It is necessary to investigate the interaction relationship between different locomotives and different traction networks.

The impedance-based method is a powerful tool to assess stability issues [17]. It was first formulated for converter-filter [18] and general source-load [19]–[22] interaction problems in DC power electronic systems. Later, it was derived for three-phase AC systems, such as grid-connected inverter systems [23], distributed power systems [24] and converter-filter systems [25]. In three-phase systems, the AC operation point can be transformed into a DC one by *dq* decomposition. Then the stability analysis can be carried out by applying criteria to the *dq*-frame impedance which is obtained by the small-signal method near the DC equilibrium point. As an interaction system of locomotive and traction network, the stability of the L-N system also can be studied by the impedance-based method.

The L-N system, however, is single-phase. The difficulty of the impedance modeling is how to linearize the single-phase converter in a locomotive. One kind of controller, the *dq* current control, is used in some types of locomotives by constructing a fictitious β axis lagging the original signal by 90°, although there is only one phase in the electric railway [15], [26]. And some blocks, such as *dq* transformations and second order generalized integrators, are borrowed from three-phase systems to control active and reactive power independently. Consequently, it is convenient to derive the *dq*-frame impedance model by the similar method which has been applied to the three-phase systems [27]. Another kind of converter controller, the transient current control algorithm (TCCA), is also widely used in locomotives due to fast current feedback and strong robustness [28], [29]. In contrast to the *dq* current control, the inputs and outputs of controllers are not transformed into *dq*-frame signals in TCCA. When applying the *dq*-frame impedance-based method to the L-N system, this paper will focus on deriving the *dq*-frame impedance of this controller.

The rest of this paper is organized as follows: In Section II, the typical characteristic of HOHR is introduced through measured data in an electric railway. In Section III, the impedance models of traction networks and locomotives are derived respectively. Then in Section IV the stability of the L-N system is assessed at the hand of a bode diagram of the impedance model when there are different traction networks and locomotives. Further, a time-domain simulation study is conducted to validate the analytical model. In Section V, the field test data from an electric railway is used to validate the stability analysis results. Finally, Section VI summarizes and concludes the paper.

This paper derives not only the *dq*-frame impedance model of the converter with TCCA but also the detailed impedance model of a traction network with distributed parameters. The stability of L-N systems can be assessed through the bode diagrams of the locomotives impedance and traction networks impedance separately. As a result, HOHR can be predicted before a new type of locomotive is put into use.

II. HIGH-ORDER HARMONIC RESONANCE OF LOCOMOTIVE-NETWORK SYSTEM

In the L-N system of the electric railway, the locomotive is a typical harmonic source due to its AC-DC-AC traction drive system, which injects harmonics into the traction network during the normal operation of the interaction system, as shown in Fig. 1. Three-phase power grid provides electric power for the railway. A substation transfers three-phase electric power into single-phase electric power which is required by the traction network. The locomotive's traction drive system is divided into five parts: The traction transformer, the AC/DC converter, the DC link, the DC/AC inverter, and motors. In Fig.1, i_{h2} refers to the harmonic current that is generated by locomotive's traction drive system, and i_h to the harmonic current injected into primary winding, which
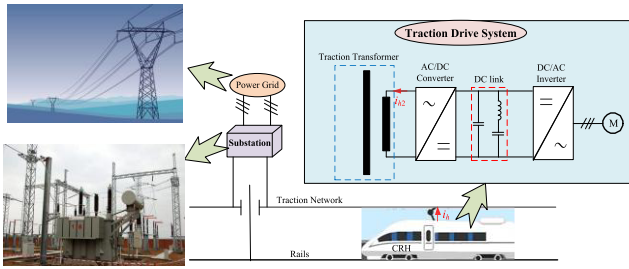
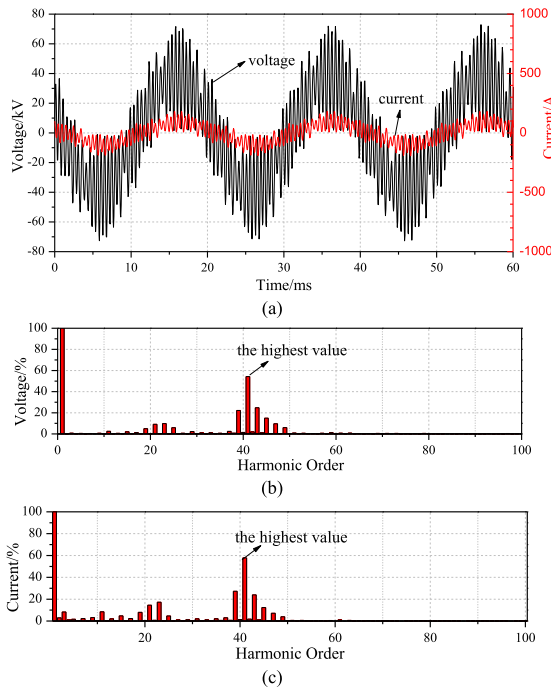**FIGURE 1.** Structure diagram of locomotive-network interacted system.

FIGURE 2. Field test result of HOHR: (a) waveforms of voltage and current, (b) spectrum of voltage, (c) spectrum of current.

circulates in the traction network. If harmonic current and harmonic voltage are amplified due to the interaction between the locomotive and traction network, HOHR will occur within the L-N system.

Figure 2 illustrates the field test results when HOHR occurs. The resonance frequency is 2050Hz. The voltage and current waveforms of the primary winding of the traction transformer are shown in Fig. 2(a). The fundamental voltage is 27.3kV, and the fundamental current is 59.9A. Obviously, there is a serious distortion of voltage and current. Following, the spectrums of the voltage and current are obtained by applying the Fast Fourier Transformation (FFT) to voltage data and current data. As shown in Fig. 2(b), the harmonic voltage of 2050Hz (41st) is as high as 14.8kV (54.2% of fundamental) which is the highest among all harmonic components. As shown in Fig. 2(c), the 41st harmonic current is also the highest among all harmonic components. Furthermore, the RMS (root mean square values) voltage is 33.4kV, which is far beyond the rated voltage of traction networks, which

stands at 27.5 kV. As a result, high-voltage devices may be damaged and the locomotives may even fail to function.

III. IMPEDANCE MODEL OF TRACTION NETWORKS AND LOCOMOTIVES
A. IMPEDANCE MATCHING BETWEEN LOCOMOTIVES AND TRACTION NETWORKS

When the impedance-based method is applied in order to analyze the source-load system stability, the system is represented as a closed-loop system of equivalent source impedance and equivalent load impedance. The system stability is then evaluated by studying the open-loop gain of the closed-loop system. In an electric railway, the traction network provides electricity for the locomotive. That is to say, the traction network is the power source, and the locomotive is the load.
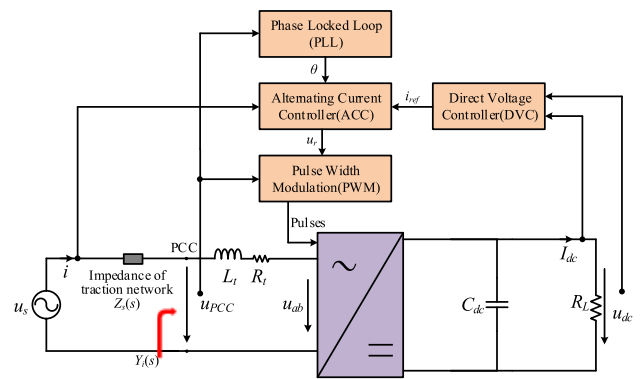

FIGURE 3. Schematic diagram of impedance matching relation.

As shown in Fig. 3, traction networks and locomotives are connected at a point of common coupling (PCC). It should be noted that locomotives' traction transformer is excluded because the voltage of the traction network has been transferred to the voltage of the secondary winding of the traction transformer. The traction network is equivalent to the impedance, $Z_s(s)$, which differs from the resistance-inductance in series circuit. It is influenced by the total length of the network and the location of the locomotive. L_t and R_t are the equivalent inductance and resistance of the traction transformer, respectively.

The control blocks of the PWM converter contain phase locked loop (PLL), a direct voltage controller (DVC), an alternating current controller (ACC), and a pulse width modulator (PWM). If we ignore the DVC, PLL and PWM, an analytical model is then given by

$$i = G_{ci}(s) i_{ref} + Y_i(s) u_{PCC} \qquad (1)$$

where $G_{ci}(s)$ is the closed-loop transfer function of ACC, and $Y_i(s)$ is the input admittance of the PWM converter.

In the circuit of traction network and PWM converter, the u_{PCC} is

$$u_{PCC} = u_s - Z_s(s) i \qquad (2)$$

where u_s is the ideal voltage source.

Equation (2) is then substituted into (1) and the resulting expression for *i* is:

$$i = \frac{1}{1 + Y_i(s) Z_s(s)} \left[G_{ci}(s) i_{ref} + Y_i(s) u_s \right] \quad (3)$$

The small-signal method is adopted around the steady-state operation point, and thus the expression for the linearized system is

$$\Delta i = \frac{1}{1 + (Z_s(s) / Z_i(s))} Y_i(s) \Delta u_s \quad (4)$$

where $Z_i(s)$ is the input impedance of the PWM converter and $Z_i(s) = 1/Y_i(s), Z_s(s) = 1/Y_s(s)$.
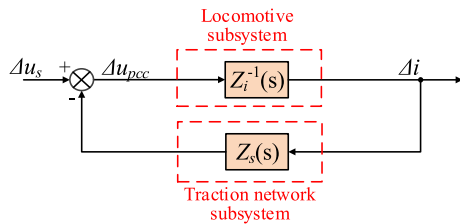

FIGURE 4. Closed-loop structure of the locomotive-network system.

According to (4), the L-N system resembles a closed-loop system, as shown in Fig. 4. An input signal passes through $Y_i(s)$ to give an output which is then fed back through $Z_s(s)$. Therefore, the stability of locomotive-network system can be studied by applying the Nyquist stability criterion to the closed-loop system of the traction network impedance (Z_s) and the locomotive impedance (Z_i).

B. IMPEDANCE MODEL OF TRACTION NETWORKS

The traction network is a complicated system with distributed parameters. The impedance varies with the total length of the network and the location of the locomotive. Therefore, the impedance model of the traction network cannot be simply equivalent to a lumped-parameter circuit. Compared with resistance-inductance equivalent, the impedance model of the traction network is derived through taking the distributed structure into consideration.
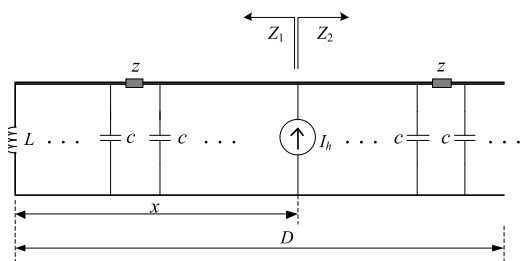

FIGURE 5. The distributed structure of the traction network.

The distributed structure of the traction network is shown in Fig. 5. The locomotive's PWM converter is regarded as a harmonic current source, I_h, where h represents the harmonic order. L is the equivalent inductance (without regard to the

resistance) of the traction power supply system including the substation and power grid. The network is substituted by the conductor with distributed parameters in which c is the parallel capacitance and z is the series impedance per unit length. D is the total length from the substation to the section post, and x is the distance from the substation to the location of the locomotive. Z_1 is the impedance which is seen from the locomotive to the substation and Z_2 is the impedance which is seen from the locomotive to the section post.

The parallel impedance of the left and right side is calculated as [9]

$$Z_s = \frac{Z_1 Z_2}{Z_1 + Z_2} = Z_c ch\gamma (D - x) \frac{j\omega Lch(\gamma x) + Z_c sh(\gamma x)}{j\omega Lsh(\gamma D) + Z_c ch(\gamma D)}$$

where Z_c is the characteristic impedance of the equivalent single-phase line, and γ is the propagation constant of the equivalent single-phase line. For values, there are $Z_c = \sqrt{z/(j\omega c)}$ and $\gamma = \sqrt{j\omega cz}$, where ω is angular frequency.
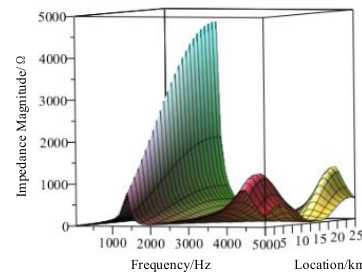

FIGURE 6. Calculation result of impedance for traction network when the location of the locomotive changes.

When the location of the locomotive is different, the magnitude of Z_s is displayed in Fig. 6, where c is 17.96 nF/km, z is 0.16+j0.54 for 50Hz, L is 15.76mH for 50Hz, and D is 25km. Obviously, there are two peak points of impedance magnitude at some locations. According to field test data [30], the range of the resonance frequency is 750∼3500Hz. So the first peak point needs to be taken into consideration while the second peak point peak is ignored. When the location is further away, the impedance peak is higher. The frequency of the peak point is not, however, influenced by the location of the locomotive. Consequently, the impedance-frequency characteristic of the traction network is different from that of a lumped parameter circuit. When we derive the impedance model of the traction network, the complicated structure and distributed parameters should be considered.

The simulation model is then established using Matlab/Simulink software. The total length of the feeding post is divided into several units which are modeled as several cells of a multi-conductor transmission line. The cell model is illustrated in Fig. 7. The model includes the line-line and line-ground capacitance, as well as the mutual impedance of line and line-line. The simulation results are depicted in Fig. 8. Obviously, there is a resonance frequency of the traction network, as with the mathematical analysis in Fig. 6.
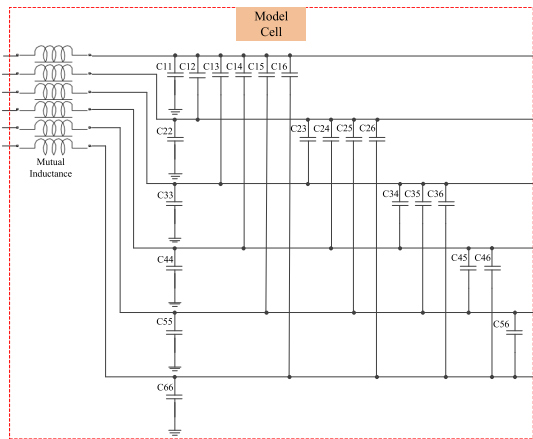
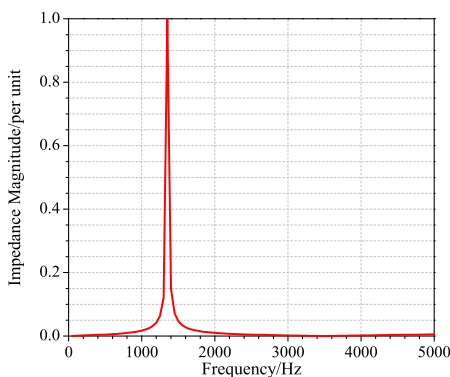**FIGURE 7.** Simulink model of the traction network.

FIGURE 8. Simulink result of the impedance in traction network.

To acquire reliable test data, this paper adopts a laboratory-scale harmonic generator [31] which can be installed between the contact line and the rails. The rated power of the equipment is 150kVA and the rated voltage is 25kV. The key component of this equipment is the single-phase cascaded H-bridge which can generate high-order harmonics ranging from 50Hz to 5000Hz by designing effective control strategies.
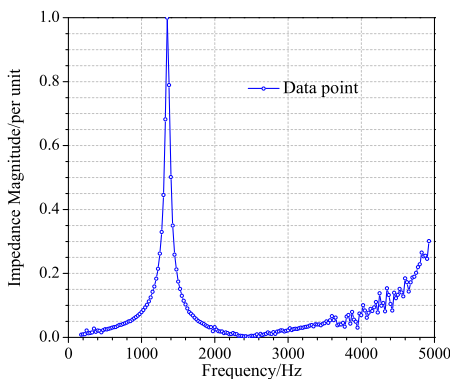

FIGURE 9. Measurement result of impedance in real traction network.

The measurement results for a real traction network are depicted in Fig. 9. The impedance characteristic is obtained through the data points. The test section is from the

Substation A to the Substation B of the Beijing-Shenyang Passenger Dedicated Line. The total length of the feeding post from the substation to the section post is 24.65km. The location of the equipment is the middle point of the whole feeding section. As shown in Fig. 9, there is a peak point at 1350Hz and the impedance magnitude is 1221.7Ω. That is, the natural resonance frequency is 1350Hz.

The extreme point is the noticeable feature in both Fig. 8 and Fig. 9. With respect to peak points, the simulation results fit the theoretical analysis results and field test result well. Moreover, the peak point of the impedance-frequency characteristic curve is a key factor in analyzing the HOHR problem. Hence, the multi-conductor model in this paper is effective for exploring the influence of the traction network on HOHR. It is not always feasible to conduct a field test of an electric railway, so the impedance model of the traction network can be obtained by the simulation model which is able to take the distributed structure into account.

C. IMPEDANCE MODEL OF LOCOMOTIVES

The L-N system is a typical single-phase system, in which the PWM converter of the locomotive interacts with the traction network, sometimes resulting in HOHR. It is thus necessary to obtain the impedance of the converter. The converter's controller is important for impedance modeling. TCCA is widely used in the locomotives' converters. The control structure of TCCA is shown in Fig. 10. In the double closed-loop control, the outer voltage control loop provides the reference value for the inner current control loop and keeps the DC voltage stable. The inner current control outputs the modulation wave and maintains the current according to the reference value.

In order to derive the analytical impedance model of the locomotive (mainly the PWM converter), a small-signal method is applied around the steady-state equilibrium point to linearize the PWM converter. The impedance derivation is given in more detail below.

The SOGI-PLL block transfers the sing-phase voltage of the electric railway into an orthogonal voltage system based on second order generalized integrators (SOGI) [32]. There exists a difference between the phase detected by PLL, θ, and the actual phase of the voltage, θ_0, due to sample delay, digital controls, and small-signal disturbances while the AAC block adopts the PLL phase. There are thus two systems: The controller signal system and the power stage source signal system, represented by superscript c and s respectively. A small variation, namely $\Delta\theta$ ($\Delta\theta = \theta - \theta_0$), is introduced into the small-signal method for deriving the impedance model of PWM converter [9], [15], [33].

Note that SOGI generates the d-axis and q-axis of the voltage and PLL closely links with e_q. Accordingly, the quantities of DVC and ACC are converted into dq-axis forms in a synchronous reference ($d-q$) frame with subscript d and q respectively. The steady-state equilibrium point is given by a capital letter. As a result, all the quantities are transferred into DC quantities.
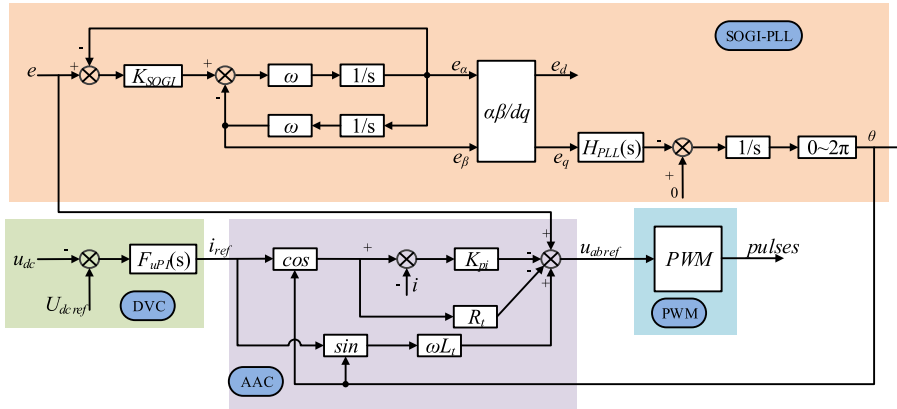
FIGURE 10. Block diagram of the transient current control algorithm.

The voltage relationship between the converter signal system and the source signal system can be expressed as

$$E^c = e^{-j\Delta\theta} E^s \qquad (5)$$

where $E^c = \begin{bmatrix} e_d^c & e_q^c \end{bmatrix}^T$ and $E^s = \begin{bmatrix} e_d^s & e_q^s \end{bmatrix}^T$.

Small-signal variables are then introduced into (5) which yields:

$$\Delta\theta = \frac{H_{PLL}}{s + E_d^s H_{PLL}} \Delta e_q^s = G_{PLL} \Delta e_q^s \qquad (6)$$

The modulation wave signal u_{abref} generated by ACC is given by the relational expression including inputs and outputs

$$u_{abref} = e + \omega L_t i_{ref} \sin\theta - R_t i_{ref} \cos\theta - K_{pi} \left(i_{ref} \cos\theta - i \right) \qquad (7)$$

Applying dq-transformation into e, i, u_{abref}, and i_{ref}, we obtain

$$\begin{bmatrix} \Delta u_{abdref} \\ \Delta u_{abqref} \end{bmatrix} = \begin{bmatrix} 1 & \omega L_t I_{dref}^0 G_{PLL} \\ 0 & 1 - \left(R_t + K_{pi} \right) I_{dref}^0 G_{PLL} \end{bmatrix} \begin{bmatrix} \Delta e_d \\ \Delta e_q \end{bmatrix}$$
$$- \begin{bmatrix} K_{pi} & 0 \\ 0 & K_{pi} \end{bmatrix} \begin{bmatrix} \Delta i_{dref} - \Delta i_d \\ \Delta i_{qref} - \Delta i_q \end{bmatrix}$$
$$- \begin{bmatrix} R_t & 0 \\ \omega L_t & 0 \end{bmatrix} \begin{bmatrix} \Delta i_{dref} \\ \Delta i_{qref} \end{bmatrix} \qquad (8)$$

where I_{dref}^0 and I_{qref}^0 are the steady-state value of i_{dref} and i_{qref} respectively.

Equation (8) also can be written into matrix form:

$$\Delta u_{abref} = H_{abe} \Delta e - H_{abpi} \left(\Delta i_{ref} - \Delta i \right) - H_{abref} \Delta i_{ref} \qquad (9)$$

The dynamic relationship of the PWM converter can be found by applying the Kirchhoff Voltage Law (KVL) to the equivalent circuit of Fig. 3

$$e = L_t \frac{di}{dt} + R_t i + u_{ab} \qquad (10)$$

Next, by Laplace's Transformation, the small-signal frequency-domain equation is represented as:

$$\Delta i = H_{RL} \left(\Delta e - \Delta u_{ab} - H_L \Delta i \right) \qquad (11)$$

where $H_{RL} = \begin{bmatrix} \frac{1}{R_t + sL_t} & 0 \\ 0 & \frac{1}{R_t + sL_t} \end{bmatrix}$, $H_L = \begin{bmatrix} 0 & -\omega L_t \\ \omega L_t & 0 \end{bmatrix}$.

The PWM process can be equivalent to [34]

$$\Delta u_{ab} = G_{PWM} \Delta u_{abref} \qquad (12)$$

where $G_{PWM} = \begin{bmatrix} \frac{1}{T_d s + 1} & 0 \\ 0 & \frac{1}{T_d s + 1} \end{bmatrix}$, Td denotes the time delay.

Inserting (9) and (12) into (11), equation (11) becomes into another form:

$$\Delta i = G_{ie} \Delta e + G_{iref} \Delta i_{ref} \qquad (13)$$

where I am the 2×2 identity matrix,

$$G_{ie} = \left(I + H_{RL} G_{PWM} H_{abpi} + H_{RL} H_L \right)^{-1}$$
$$\times H_{RL} \left(I - G_{PWM} H_{abe} \right)$$

and

$$G_{iref} = \left(I + H_{RL} G_{PWM} H_{abpi} + H_{RL} H_L \right)^{-1}$$
$$\times H_{RL} G_{PWM} \left(H_{abpi} + H_{abref} \right).$$

For an ideal voltage source rectifier (VSR), the power is balanced between the AC-side and the DC-side of the H-bridge. Accordingly, for occasions of rated power, the reference of the ACC can be obtained based on the small-signal method

$$\begin{bmatrix} \Delta i_{dref} \\ \Delta i_{qref} \end{bmatrix} = \begin{bmatrix} -\frac{I_{d0} F_{uPI}}{s C_{dc} U_{dc0}} & 0 \\ 0 & 0 \end{bmatrix} \begin{bmatrix} \Delta e_d \\ \Delta e_q \end{bmatrix}$$
$$+ \begin{bmatrix} -\frac{E_{d0} F_{uPI}}{s C_{dc} U_{dc0}} & 0 \\ 0 & 0 \end{bmatrix} \begin{bmatrix} \Delta i_d \\ \Delta i_q \end{bmatrix} \qquad (14)$$

where I_{d0}, E_{d0}, and U_{dc0} are the steady-state values of i, e, and u_{dc} respectively.
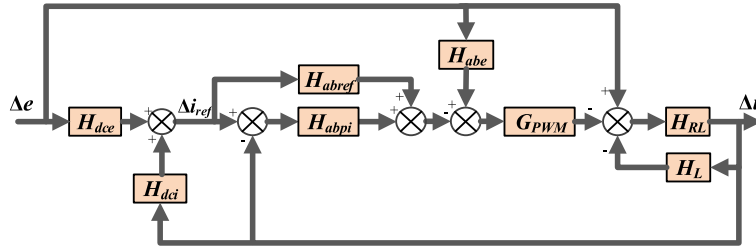
FIGURE 11. Block diagram of the controller in small-signal system.

Equation (14) can also be written as:

$$\Delta i_{ref} = H_{dce} \Delta e + H_{dci} \Delta i \tag{15}$$

The control loop of the PWM converter in the small-signal system described by (9) and (11) is depicted in Fig. 11.

Combining (13) and (15), the relationship between the current and voltage can be derived as

$$\Delta e = \left(G_{ie} + G_{iref} H_{dce} \right)^{-1} \left(I - G_{iref} H_{dci} \right) \Delta i$$

Therefore, the *dq*-frame impedance of the PWM converter is

$$Z_i = \left(G_{ie} + G_{iref} H_{dce} \right)^{-1} \left(I - G_{iref} H_{dci} \right) \tag{16}$$

According to (16), Z_i is a 2×2 diagonal matrix due to the *dq*-decoupling method applied into a single-phase control strategy (not the *dq*-frame control strategy). Also, to achieve a unity power factor, it is recommended to set *q*-axis current reference of the PWM converter of the locomotive to zero. As a result, the influence of off-diagonal elements on the stability assessment is negligible. That is to say, perturbation in one channel only induces a response in the same channel. The impedance matrix of the locomotive can be given as:

$$Z_i = \begin{bmatrix} Z_{idd} & 0 \\ 0 & Z_{iqq} \end{bmatrix}$$

Furthermore, the frequency responses of the diagonal elements, Z_{idd} and Z_{iqq}, are influenced by main circuit parameters and the controller parameters of the PWM converter. Generally, different types of locomotives have different parameters. As a result, the impedance characteristics differ between different locomotives.
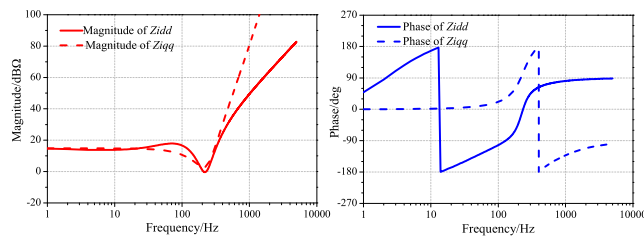

FIGURE 12. Impedance frequency response predicted by (16).

The frequency responses of Z_{idd} and Z_{iqq} are presented in Fig. 12 for the parameters listed in Table 2, found in Appendix A. As shown in Fig. 12, there is no negative

magnitude (in dB) of Z_{idd} and Z_{iqq}. Moreover, the magnitudes of Z_{idd} and Z_{iqq} are nearly invariable at frequencies below 50Hz. On the other hand, at high frequencies above 150Hz, both of these impedance magnitudes increase dramatically. Therefore, when researching the locomotive impedance for stability analysis of the L-N system, we cannot simply consider the PWM converter as an equivalent inductance.

IV. HIGH-ORDER HARMONIC RESONANCE ANALYSIS BASED ON IMPEDANCE SPECIFICATIONS OF L-N SYSTEMS

A. STABILITY CRITERION BASED-ON IMPEDANCE MODEL

The impedance-based stability criterion is based on the closed-loop system where the forward gain is load admittance $Z_i^{-1}(s)$ and the feedback gain is source impedance $Z_s(s)$. Phase margin (PM) is defined as the amount of change in open-loop phase needed to make a closed-loop system unstable. Specifically, the closed-loop system is unstable if the PM is negative [34], [35].

PM is the difference in phase between $-180°$ and the phase at the gain cross-over frequency that gives a gain of 0 dB [36]. So the magnitude-frequency and phase-frequency characteristics of the open-loop gain are needed to obtain PM.

For the closed-loop structure of the locomotive-network system in Fig. 3, the open-loop gain is:

$$L_{ol} = Z_i^{-1}(s) Z_s(s) = \frac{Z_s(s)}{Z_i(s)}$$

The magnitude-frequency and phase-frequency characteristics of the open-loop gain under logarithmic coordinate can be formulated as:

$$\begin{cases} A(\omega) = 20 \log |L_{ol}(\omega)| = 20 \log \left| \dfrac{Z_s(\omega)}{Z_i(\omega)} \right| \\ \qquad = A_{Zs}(\omega) - A_{Zi}(\omega) \\ \varphi(\omega) = \angle L_{ol}(\omega) = \angle \dfrac{Z_s(\omega)}{Z_i(\omega)} \\ \qquad = \angle Z_s(\omega) - \angle Z_i(\omega) = \varphi_{Zs}(\omega) - \varphi_{Zi}(\omega) \end{cases}$$

Based on the PM definition, the PM of the locomotive-network system is obtained as

$$\begin{aligned} PM &= \varphi(\omega_c) - (-180°) = 180° + \varphi(\omega_c) \\ &= 180° + \angle Z_s(\omega_c) - \angle Z_i(\omega_c) \end{aligned}$$

where $A_{Zs}(\omega_c) = A_{Zi}(\omega_c)$.

If $A_{Zs}(\omega_c) = A_{Zi}(\omega_c)$, there exists an intersection point between the magnitude-frequency curves of $Z_s(s)$ and $Z_i(s)$ in the bode diagram. As a result, the frequency characteristic of the open-loop gain is converted into frequency characteristics of $Z_s(s)$ and $Z_i(s)$ respectively. Hence PM can be obtained by calculating the phase difference between the phase-frequency curves of $Z_s(s)$ and $Z_i(s)$ at the frequency where a magnitude intersection point appears. The stability of the closed-loop system can be determined by PM at the magnitude intersection point in bode diagrams of $Z_s(s)$ and $Z_i(s)$.

The dq-frame impedance of the locomotive is a 2×2 diagonal matrix, so there are two open-loop gains for two closed-loop systems: Impedance ratios of d-channel (Z_s/Z_{idd}) and q-channel (Z_s/Z_{iqq}). The open-loop gain of the L-N system can be given as

$$L_{ol} = \begin{bmatrix} Z_s/Z_{idd} & 0 \\ 0 & Z_s/Z_{iqq} \end{bmatrix} \qquad (17)$$

Without coupled impedance, system stability is directly judged by the ratio of Z_s to Z_{idd} and the ratio of Z_s to Z_{iqq}. The AC system becomes two decoupled DC systems. Therefore, the impedance analysis methods proposed in DC systems can be applied in these two DC systems respectively [37]. The PM can be obtained by the frequency characteristics of these two open-loop gains. Consequently, the occurrence of HOHR is evaluated though phase margins for the two open-loop gains.

Instead of frequency responses (common bode diagrams) for the complete open-loop gain, it is convenient to calculate the PM by only plotting the individual frequency responses of Z_s and Z_i (including Z_{idd} and Z_{iqq}).

TABLE 1. Cases of different locomotives and traction networks.

Case	Type of locomotive	Traction network
1	Type A	Source power is 800MVA.
2	Type A	Source power increases to 1500MVA.
3	Type B	Source power is 800MVA.

Note: Both Type A locomotive and Type B locomotive have been put to use in the real electric railway

B. ASSESSMENT ON HIGH-ORDER HARMONIC RESONANCE

High-order harmonic resonance is caused by system instability. The system stability relates to the impedance characteristics of the locomotives and the traction network. As different types of locomotives are put into operation in new railway lines, the stability performance of the L-N system becomes complex. As presented in Table 1, three cases are studied in order to analyze the occurrence of HOHR in different locomotive-network systems. In these three cases, the locomotives' converters have the same controller strategy but with different proportional-integral (PI) parameters and electrical parameters as listed in Table 2, found in Appendix A.
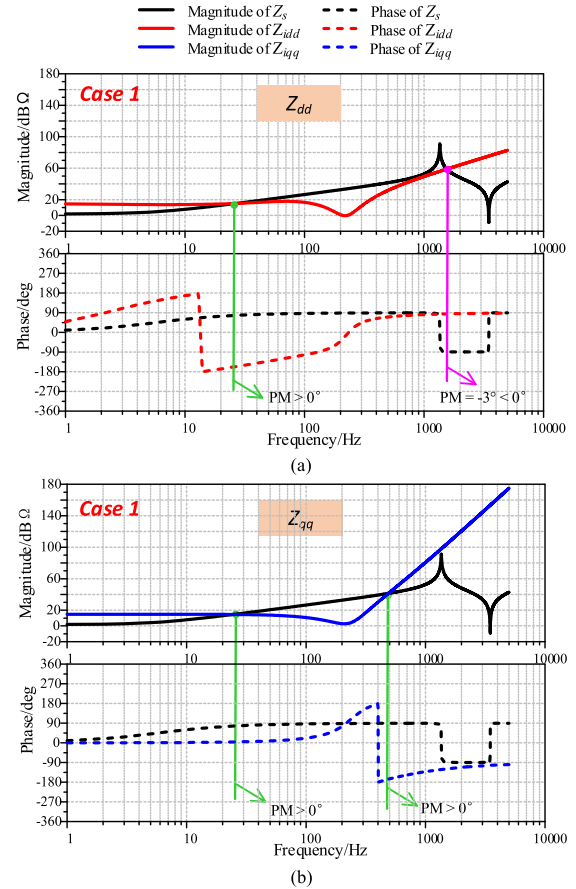

FIGURE 13. Frequency responses of Type A locomotive impedance and traction network impedance in Case 1: (a) Z_{idd} and Z_s; (b)Z_{iqq} and Z_s.

Figure 13 depicts the frequency responses of Type A locomotive impedance and network impedance in *Case* 1. Type A locomotives belong to HXD serial locomotives which are widely used in Chinese general speed railway. The parameters are listed in Table 2 in Appendix A.

As shown in Fig. 13(a), there are two magnitude intersection points of Z_{idd} and Z_s. One point locates in low frequency of 25Hz, while the other locates in a high frequency of 1450Hz. The frequency of the first intersection point is beyond the frequency range of HOHR. Further, the PM at 25Hz is positive. Therefore, the intersection point at 25Hz will not give rise to HOHR. However, the PM at 1450Hz is a negative value, −3°, which indicates the occurrence possibility of HOHR. Obviously, the impedance of the traction network at 1450Hz is close to the maximum magnitude. In addition, the frequency responses of Z_{iqq} and Z_s are displayed in Fig. 13(b). Two magnitude intersection points locate in 25Hz and 490Hz respectively and both have a positive PM. These two frequencies are beyond the frequency range of HOHR. Consequently, the magnitude intersection points of Z_{iqq} and Z_s can be ignored. For the frequency responses of Z_{idd} and Z_s, we do not need to take the intersection points at low frequency into account.

Then, to validate the theoretical analysis results of *Case* 1 based on PM criterion, the time-domain simulation model is
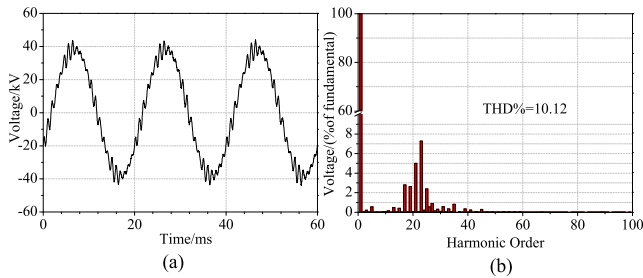
FIGURE 14. Simulation result of the Type A locomotive and the traction network in Case 1: (a) voltage waveform of u$_{PCC}$; (b) harmonic spectrum of u$_{PCC}$.

established with Matlab/Simulink software. The simulation results of *Case* 1 are given in Fig. 14. As shown in Fig. 14(a), there is obvious distortion in the voltage waveform of u_{pcc}, the voltage at PCC (point of common coupling). According to the harmonic spectrum in Fig. 14(b), the total harmonic distortion (THD) of u_{pcc} is as high as 10.12% which is much higher than that of the system without HOHR. Furthermore, the harmonic voltage at 1150Hz is the highest among all harmonic components. At 1150Hz, the harmonic content is as high as 7.27% of the fundamental.

Not surprisingly, there is a small difference between the theoretical analysis results and the simulation results of the resonance frequency, mainly because it is much more difficult to obtain the entirely accurate impedance of the traction network through the *impedance analyzer* of *powergui* block in Matlab/Simulink. Although there is a small difference, the theoretical analysis makes it possible to take precautions to avoid the occurrence of HOHR when a new electric railway is put into use.

If the traction networks or the locomotives change, the system stability will be different. The influence of traction networks and locomotives can be analyzed by comparing the impedance characteristics in three cases.

1) INFLUENCE OF TRACTION NETWORK PARAMETERS COMPARISON BETWEEN CASE 1 AND CASE 2

For heavy haul railway lines, the length of the feeding section and the conductor type of lines are almost all the same even in different lines. But the power capacity may be different for railways with different traffic volumes. The source power of the traction network increases from 800MVA in *Case*1 to 1500MVA in *Case* 2.

According to the foregoing analysis on *Case* 1, the magnitude intersection points in the frequency response of Z_{qq} have an empty effect on the occurrence of HOHR. So Fig. 15 only displays the frequency responses of Z_{dd} for Type A locomotive impedance and the traction network impedance in *Case* 2. The frequency at magnitude intersection points increases to 1850Hz. The magnitude of the traction network at 1850Hz is close to the maximum. The PM of this point is 168°. Based on PM criterion, HOHR will not occur due to positive PM.

In addition, the time-domain simulation model of *Case* 2 is also established for the new traction network.
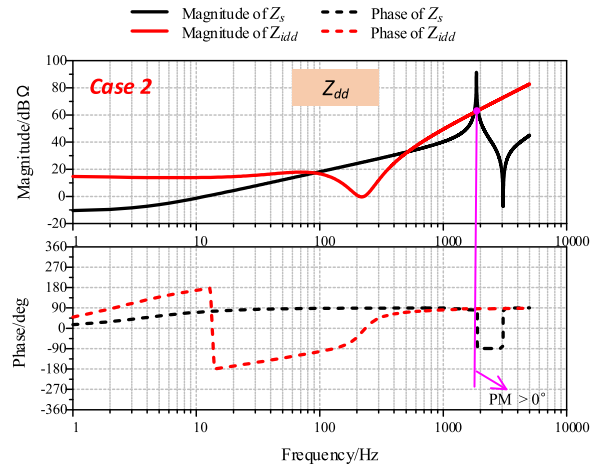

FIGURE 15. Frequency responses of Z$_{dd}$ for Type A locomotive and traction network in Case 2 with changed traction network.
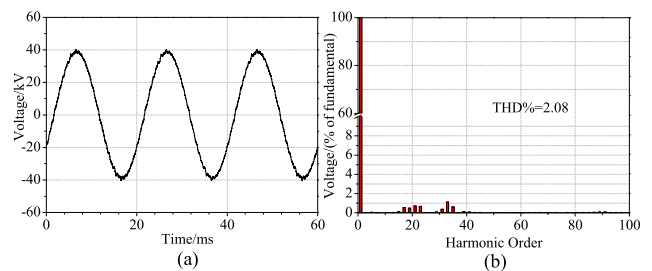

FIGURE 16. Simulation result of the Type A locomotive and the traction network in Case 2: (a) voltage waveform of u$_{PCC}$; (b) harmonic spectrum of u$_{PCC}$.

The voltage waveform and the harmonic spectrum are given in Fig. 16(a) and (b) respectively. There is no distortion of the voltage waveform. And the THD of voltage is only 2.08%, which is much lower than that of Fig. 14(b).

Namely, when the same type of locomotive connects different traction networks, although an intersection point around the maximum impedance of traction network there is, HOHR does not occur due to a positive PM.

2) INFLUENCE OF LOCOMOTIVE PARAMETERS COMPARISON BETWEEN CASE 1 AND CASE 3

Different types of locomotives differ in impedance characteristic. The locomotive is Type A in *Case* 1 but that is Type B in *Case* 3. The power of Type B locomotive is lower than that of Type A locomotive. And the controller parameters are also different.

Type B locomotives are another freight train which belongs to HXD serial locomotives. The parameters are listed in Table 2 in Appendix A. The frequency responses of Z_{dd} for Type B locomotives and the traction network in *Case* 3 are depicted in Fig. 17. There is an amplitude intersection point at 1350Hz. The magnitude of the traction network at 1350Hz is close to the maximum, which is similar to the characteristic of the intersection points in *Case* 1 and *Case* 2. The PM is 178°, which denotes that the system is stable.
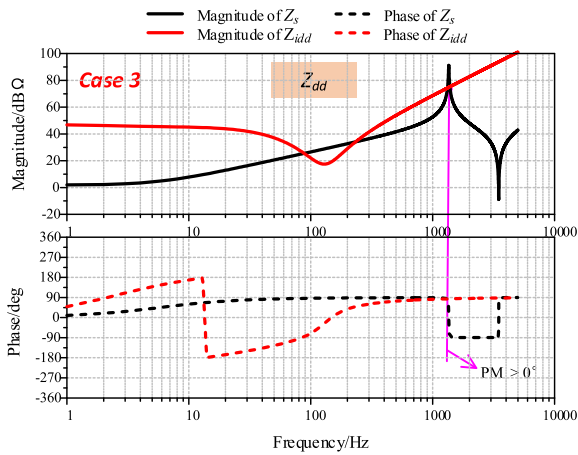
FIGURE 17. Simulation result of the Type B locomotive and the traction network in Case 3: (a) voltage waveform of u_{PCC}; (b) harmonic spectrum of u_{PCC}.
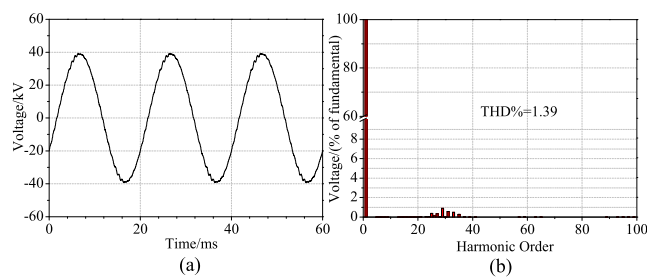

FIGURE 18. Frequency responses of Z_{dd} for Type B locomotive and traction network in Case 3 with changed locomotive.

Next, the time-domain simulation model is established in order to validate the theoretical analysis result in Fig. 17. The voltage waveform is displayed in Fig. 18(a). It can be seen that the waveform is a pure sinusoidal wave almost without distortion. Moreover, in the harmonic spectrum of Fig. 18(b), the THD is as low as 1.39%. Consequently, HOHR will not occur when Type B locomotives work in this traction network.

Above all, the occurrence of HOHR depends on not only the locomotive but also the traction network. HOHR will occur when the PM at the magnitude intersection point of Z_{idd} and Z_s is a negative value and the magnitude of the traction network at the intersection point is close to the maximum.

V. EXPERIMENT VERIFICATION BASED ON FIELD TEST

In order to validate the theoretical analysis performed through the method of PM criterion and time-domain simulation of the L-N system aforementioned, the experiment was carried out in an electric railway, Beijing-Harbin Railway.

This railway adopts the autotransformer (AT) power supply, which is comprised of contact lines, feeding lines, catenary lines, return lines, autotransformer, and rails. To date, there is barely any performance on the accurate impedance-frequency characteristic of AT traction network based on field tests. The self-developed harmonic generator was used to

conduct a field test of the traction network impedance for AT power supply in a new-built railway which has not yet been put to use. The impedance-frequency characteristic was obtained by frequency sweeping, as shown in Fig. 19. There is a peak for the impedance curve at a frequency of 850Hz.
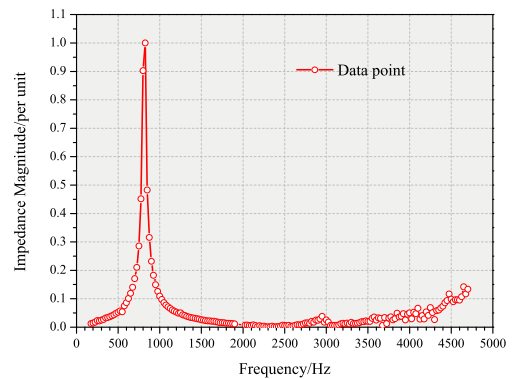

FIGURE 19. Impedance-frequency curve of traction network for AT power supply in a new-built railway.
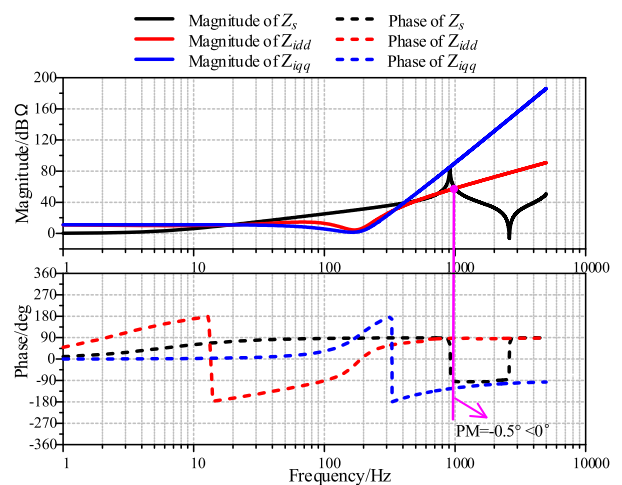

FIGURE 20. Frequency responses of Type C EMUs impedance and AT traction network impedance in Beijing-Harbin Railway.

Based on impedance characteristics of the AT traction network in the new-built line, we can obtain the impedance characteristic of Beijing-Harbin Railway which also adopts AT supply system. The stability assessment can be done by PM criterion, combined with the impedance model of Type C EMUs. Type C EMUs belong to CRH (CRH: China Railway High-speed) serial EMUs which are widely used in Chinese high-speed railway. The parameters of Type C EMUs are listed in Table 2 in Appendix A. Frequency responses of Type C EMUs impedance (Z_{idd} and Z_{iqq}) and AT traction network impedance (Z_s) are shown in Fig. 20. The intersection points located in a low-frequency range cannot give rise to HOHR. All the intersection points of Z_{iqq} and Z_s make no contribution to the occurrence of HOHR. However, there is an intersection point of Z_{idd} and Z_s at 950Hz. At that point, the PM is $-0.5°$, which indicates that HOHR is likely to occur at a frequency of 950Hz.
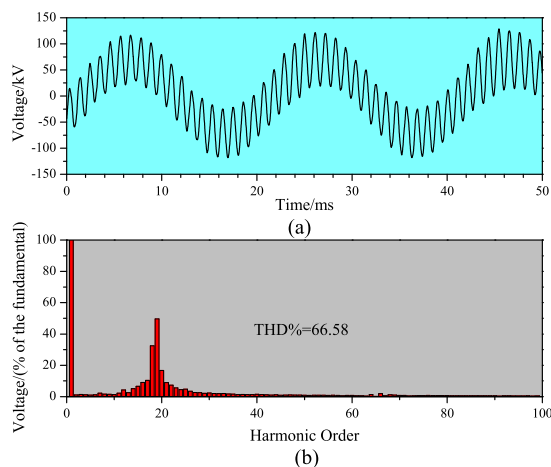
FIGURE 21. Field test result in the traction substation of Beijing-Harbin Railway: (a) voltage waveform; (b) harmonic spectrum.

The field test was carried out in a traction substation of the Beijing-Harbin Railway. As shown in Fig. 21(a), the voltage waveform presents the obvious distortion. The harmonic spectrum is displayed in Fig. 21(b). The harmonic voltage at 950Hz is the highest among all harmonic components. Apart from this, the THD is as high as 66.58%. This shows that HOHR occurs when Type C EMUs run on this line.

Overall, the field test results verify that the stability assessment based on the PM criterion is effective for predicting the occurrence of HOHR.

VI. CONCLUSION

The impedance-based method is an effective means to analyze the instability problems of an L-N system. The *dq*-frame impedance of the nonlinear converter which is controlled by TCCA is first derived through a *dq* decomposition in single-phase system. The detailed impedance of the traction network is obtained by considering all components and the distributed parameters. Then, according to the impedance-based approach, the impedance ratio of the traction network impedance to the converter impedance is the main influence factor on the stability of an L-N system. Instead of a Nyquist contour, the bode diagrams of two impedance models are applied in order to analyze the system stability. Moreover, the time-domain simulation yields the same trend as the theoretical analysis. In addition, the field test conducted on the Beijing-Harbin Railway validates the feasibility of the impedance-based method.

APPENDIX A
See Table 2.

APPENDIX B
NOMENCLATURES

| Locomotives | The trains that are used in electric railway |
| Traction network | The system providing electricity for the running locomotives |

TABLE 2. Parameters of different locomotives.

Symbol	Quantity	Value		
		Type A	Type B	Type C
u_s	Rated voltage of traction network	25kV	25kV	25kV
u_2	Rated voltage of secondary winding in traction transformer	2100V	950V	1500V
f_0	Fundamental frequency	50Hz	50Hz	50Hz
i_2	Rated current of secondary winding in traction transformer	1000A	1699A	857A
L_t	Equivalent inductance of traction transformer	2mH	0.95mH	1.2mH
R_t	Equivalent resistance of traction transformer	0.2Ω	0.2Ω	0.04Ω
C_{dc}	Capacitance of DC-link	1mF	1mF	8mF
U_{dcref}	Reference value of DVC	3775V	1800V	3000V
K_{pu}	Proportional gain of DVC	0.5	0.6	0.9
K_{iu}	Integral gain of DVC	7	15	10
K_{pi}	Proportional gain of ACC	5	7	4.3

L-N system	The coupled system of locomotive and traction network
TCCA(Transient Current Control Algorithm)	A kind of control applied in single-phase converters of locomotives
HXD	The serial locomotives which are widely used in Chinese general speed railway
CRH	The serial locomotives which are widely used in high speed railway
AT power supply	There are autotransformers in traction network

SYMBOLS

$\mathbf{Z_i}$	The impedance matrix of the locomotive converter
Z_s	The impedance of the traction network
Z_{idd}, Z_{iqq}	The diagonal elements of $\mathbf{Z_i}$
Z_{dd}	It denotes Z_{idd} and Z_s
Z_{qq}	It denotes Z_{iqq} and Z_s

REFERENCES

[1] W. Mingli, "Measurement report on abnormal fluctuation of voltage in Beijing–Guangzhou electrical railway," Beijing Jiaotong Univ., Beijing, China, Tech. Rep., 2014.

[2] C. Hengbin, S. Wensheng, G. Xinglai, and F. Xiaoyun, "High-frequency resonance suppression of high-speed railways in China," *IET Elect. Syst. Transp.*, vol. 6, no. 2, pp. 88–95, Jun. 2016.

[3] H. M. Roudsari, A. Jalilian, and S. Jamali, "Resonance assessment in electrified railway systems using comprehensive model of train and overhead catenary system," in *Proc. IEEE Int. Conf. Ind. Technol. (ICIT)*, Seville, Spain, Mar. 2015, pp. 1142–1148.

[4] E. Thunberg and L. Soder, "A Norton approach to distribution network modeling for harmonic studies," *IEEE Trans. Power Del.*, vol. 14, no. 1, pp. 272–277, Jan. 1999.

[5] X. Wang, F. Blaabjerg, and W. Wu, "Modeling and analysis of harmonic stability in an AC power-electronics-based power system," *IEEE Trans. Power Electron.*, vol. 29, no. 12, pp. 6421–6432, Dec. 2014.

[6] L. Harnefors, M. Bongiorno, and S. Lundberg, "Input-admittance calculation and shaping for controlled voltage-source converters," *IEEE Trans. Ind. Electron.*, vol. 54, no. 6, pp. 3323–3334, Dec. 2007.

[7] L. Sainz, L. Monjo, S. Riera, and J. Pedra, "Study of the Steinmetz circuit influence on AC traction system resonance," *IEEE Trans. Power Del.*, vol. 27, no. 4, pp. 2295–2303, Oct. 2012.

[8] X. Zhang, J. Chen, G. Zhang, L. Wang, R. Qiu, and Z. Liu, "An active oscillation compensation method to mitigate high-frequency harmonic instability and low-frequency oscillation in railway traction power supply system," *IEEE Access*, vol. 6, pp. 70359–70367, 2018.

[9] H. Lee, C. Lee, G. Jang, and S.-H. Kwon, "Harmonic analysis of the korean high-speed railway using the eight-port representation model," *IEEE Trans. Power Del.*, vol. 21, no. 2, pp. 979–986, Apr. 2006.

[10] H. Cui, W. Song, H. Fang, X. Ge, and X. Feng, "Resonant harmonic elimination pulse width modulation-based high-frequency resonance suppression of high-speed railways," *IET Power Electron.*, vol. 8, no. 5, pp. 735–742, May 2015.

[11] J. Li, M. Wu, and Q. Liu, "Measurement and simulation on low-frequency oscillation in the traction network of Xuzhou North Railway Hub," in *Proc. 12th World Congr. Intell. Control Automat.*, Guilin, China, Jun. 2016, pp. 1797–1802.

[12] K. Song, G. Konstantinou, W. Mingli, P. Acuna, R. P. Aguilera, and V. G. Agelidis, "Windowed SHE-PWM of interleaved four-quadrant converters for resonance suppression in traction power supply systems," *IEEE Trans. Power Electron.*, vol. 32, no. 10, pp. 7870–7881, Oct. 2017.

[13] Y. Liao, Z. Liu, H. Zhang, and B. Wen, "Low-frequency stability analysis of single-phase system withdq-frame impedance approach—Part I: Impedance modeling and verification," *IEEE Trans. Ind. Appl.*, vol. 54, no. 5, pp. 4999–5011, Oct. 2018.

[14] H. Tao, H. Hu, X. Wang, F. Blaabjerg, and Z. He, "Impedance-based harmonic instability assessment in a multiple electric trains and traction network interaction system," *IEEE Trans. Ind. Appl.*, vol. 54, no. 5, pp. 5083–5096, Sep./Oct. 2018.

[15] H. Wang, W. Mingli, and J. Sun, "Analysis of low-frequency oscillation in electric railways based on small-signal modeling of vehicle-grid system in dq frame," *IEEE Trans. Power Electron.*, vol. 30, no. 9, pp. 5318–5330, Sep. 2015.

[16] X. Zhang, L. Wang, W. Dunford, J. Chen, and Z. Liu, "Integrated full-frequency impedance modeling and stability analysis of the train-network power supply system for high-speed railways," *Energies*, vol. 11, p. 1714, Jul. 2018.

[17] B. Wen, D. Dong, D. Boroyevich, P. Mattavelli, R. Burgos, and Z. Shen, "Impedance-based analysis of grid-synchronization stability for three-phase paralleled converters," *IEEE Trans. Power Electron.*, vol. 31, no. 1, pp. 26–38, Jan. 2016.

[18] R. D. Middlebrook, "Input filter considerations in design and application switching regulators," in *Proc. IEEE Ind. Appl. Soc. Annu. Meeting*, Jan. 1976, pp. 366–382.

[19] X. Feng, J. Liu, and F. C. Lee, "Impedance specifications for stable DC distributed power systems," *IEEE Trans. Power Electron.*, vol. 17, no. 2, pp. 157–162, Mar. 2002.

[20] C. M. Wildrick, F. C. Lee, B. H. Cho, and B. Choi, "A method of defining the load impedance specification for a stable distributed power system," *IEEE Trans. Power Electron.*, vol. 10, no. 3, pp. 280–285, May 1995.

[21] X. Zhang, X. Ruan, and Q.-C. Zhong, "Improving the stability of cascaded DC/DC converter systems via shaping the input impedance of the load converter with a parallel or series virtual impedance," *IEEE Trans. Ind. Electron.*, vol. 62, no. 12, pp. 7499–7512, Dec. 2015.

[22] Y. Panov, J. Rajagopalan, and F. C. Lee, "Analysis and design of N paralleled DC-DC converters with master-slave current-sharing control," in *Proc. Appl. Power Electron. Conf.*, vol. 1, Feb. 1997, pp. 436–442.

[23] Y. Wang, X. Wang, F. Blaabjerg, and Z. Chen, "Harmonic instability assessment using state-space modeling and participation analysis in inverter-fed power systems," *IEEE Trans. Ind. Electron.*, vol. 64, no. 1, pp. 806–816, Jan. 2017.

[24] B. Wen, R. Burgos, D. Boroyevich, P. Mattavelli, and Z. Shen, "AC stability analysis and dq frame impedance specifications in power-electronics-based distributed power systems," *IEEE J. Emerg. Sel. Topics Power Electron.*, vol. 5, no. 4, pp. 1455–1465, Dec. 2017.

[25] M. Schweizer and J. W. Kolar, "Shifting input filter resonances—An intelligent converter behavior for maintaining system stability," in *Proc. Int. Power Electron. Conf. (ECCE ASIA)*, Jun. 2010, pp. 906–913.

[26] S. Danielsen, "Electric traction power system stability," Ph.D. dissertation, Norwegian Univ. Sci. Technol., Trondheim, Norway, Tech. Rep., 2010.

[27] Y. Liao, Z. Liu, H. Zhang, and B. Wen, "Low-frequency stability analysis of single-phase system withdq-frame impedance approach—Part II: Stability and frequency analysis," *IEEE Trans. Ind. Appl.*, vol. 54, no. 5, pp. 5012–5024, Oct. 2018.

[28] Z. Liu, C. Xiang, Y. Wang, Y. Liao, and G. Zhang, "A model-based predictive direct power control for traction line-side converter in high-speed railway," *IEEE Trans. Ind. Appl.*, vol. 53, no. 5, pp. 4934–4943, Sep./Oct. 2017.

[29] W. Hui, W. Mingli, G. A. Vassilios, and S. Kejian, "Steady-state harmonic domain matrix-based modeling of four-quadrant EMU line converter," *J. Power Electron.*, vol. 14, no. 3, pp. 572–579, 2014.

[30] *Report on Influence Mechanism of High-Order Harmonic for AC Locomotives*, Beijing Jiaotong Univ., Beijing, China, 2010.

[31] L. Qiujiang, W. Mingli, Z. Junqi, S. Kejian, and W. Liran, "Resonant frequency identification based on harmonic injection measuring method for traction power supply systems," *IET Power Electron.*, vol. 11, no. 3, pp. 585–592, Mar. 2018.

[32] M. Ciobotaru, R. Teodorescu, and F. Blaabjerg, "A new single-phase PLL structure based on second order generalized integrator," in *Proc. 37th IEEE Power Electron. Spec. Conf.*, Jun. 2006, pp. 1–6.

[33] B. Wen, D. Boroyevich, R. Burgos, P. Mattavelli, and Z. Shen, "Analysis of D-Q small-signal impedance of grid-tied inverters," *IEEE Trans. Power Electron.*, vol. 31, no. 1, pp. 675–687, Jan. 2016.

[34] X. Wang, L. Harnefors, and F. Blaabjerg, "Unified impedance model of grid-connected voltage-source converters," *IEEE Trans. Power Electron.*, vol. 33, no. 2, pp. 1775–1787, Feb. 2018.

[35] Z. Liu, G. Zhang, and Y. Liao, "Stability research of high-speed railway EMUs and traction network cascade system considering impedance matching," *IEEE Trans. Ind. Appl.*, vol. 52, no. 5, pp. 4315–4326, Sep./Oct. 2016.

[36] S. Kim, *Electric Motor Control*. Amsterdam, The Netherlands: Elsevier, 2017.

[37] B. Wen, D. Boroyevich, R. Burgos, P. Mattavelli, and Z. Shen, "D-Q impedance specification for balanced three-phase AC distributed power system," in *Proc. IEEE Appl. Power Electron. Conf. Expo. (APEC)*, Mar. 2015, pp. 2757–2771.

JING LI received the B.Sc. degree in electrical engineering from the North China University of Water Resources and Electric Power, Zhengzhou, China, in 2013, and the M.Sc. degree from Beijing Jiaotong University, Beijing, China, in 2016, where she is currently pursuing the Ph.D. degree in electrical engineering. Her research interests include power quality of electric railways and power electronics in power supply systems.

MINGLI WU was born in Hebei, China. He received the B.Sc. and M.Sc. degrees in electrical engineering from Southwest Jiaotong University, Chengdu, China, in 1993 and 1996, respectively, and the Ph.D. degree in electrical engineering from Beijing Jiaotong University, Beijing, China, in 2006, where he has been a Professor with the School of Electrical Engineering, since 2008. His research interests include power supply for electric railways, digital simulation of power systems, and electric power quality.

MARTA MOLINAS (M'94) received the Diploma degree in electromechanical engineering from the National University of Asuncion, Asuncion, Paraguay, in 1992, the M.Eng. degree in information engineering from Ryukyu University, Nishihara, Japan, in 1997, and the D.Eng. degree in electrical engineering from the Tokyo Institute of Technology, Tokyo, Japan, in 2000.

She was a Guest Researcher with the University of Padova, Italy, in 1998. From 2004 to 2007, she was a Postdoctoral Researcher with the Norwegian University of Science and Technology (NTNU), Trondheim, Norway, where she has been a Professor with the Department of Electric Power Engineering, from 2008 to 2014. She is currently a Professor with the Department of Engineering Cybernetics, NTNU. Her research interests include the stability of complex power electronics systems, harmonics, oscillatory phenomena, and nonstationary signals from the human and the machine. She serves as an Editor for the IEEE JOURNAL OF EMERGING AND SELECTED TOPICS IN POWER ELECTRONICS and the IEEE TRANSACTIONS ON ENERGY CONVERSION. She is an Associate Editor of the IEEE TRANSACTIONS ON POWER ELECTRONICS and the IEEE TRANSACTIONS ON INDUSTRIAL ELECTRONICS.

KEJIAN SONG was born in Hunan, China, in 1988. He received the B.Sc. degree in electrical engineering from Shaoyang University, Shaoyang, China, in 2010, the M.Sc. and Ph.D. degrees in electrical engineering from Beijing Jiaotong University (BJTU), Beijing, China, in 2012 and 2017, respectively, where he is currently a Postdoctoral Researcher. From 2014 to 2015, he was with the Australia Energy Research Institute, UNSW Sydney, Australia, as an exchanged Ph.D. student sponsored by the China Scholarship Council. His research interests include modulation methods and control strategies for traction converters and electric power quality of traction power supply systems.

QIUJIANG LIU was born in Hebei, China. He received the B.Sc., M.Sc., and Ph.D. degrees in electrical engineering from Beijing Jiaotong University, Beijing, China, in 2012, 2014, and 2016, respectively. His research interests include power quality of electric railways and power electronics in power supply systems.

● ● ●